α-Synuclein Multistate Folding Thermodynamics: Implications for Protein Misfolding and Aggregation[†]

Allan Chris M. Ferreon and Ashok A. Deniz*

Department of Molecular Biology, The Scripps Research Institute, 10550 North Torrey Pines MB-19, La Jolla, California 92037

Received November 29, 2006; Revised Manuscript Received February 16, 2007

ABSTRACT: α-Synuclein aggregation has been tightly linked with the pathogenesis of Parkinson's disease and other neurodegenerative disorders. Despite the protein's putative function in presynaptic vesicle regulation, the roles of lipid binding in modulating α-synuclein conformations and the aggregation process remain to be fully understood. This study focuses on a detailed thermodynamic characterization of monomeric α-synuclein folding in the presence of SDS, a well-studied lipid mimetic. Far-UV CD spectroscopy was employed for detection of conformational transitions induced by SDS, temperature, and pH. The data we present here clearly demonstrate the multistate nature of α-synuclein folding, which involves two predominantly α-helical partially folded thermodynamic intermediates that we designate as F (most folded) and I (intermediately folded) states. Likely structures of these α-synuclein conformational states are also discussed. These partially folded forms can exist in the presence of either monomeric or micellar forms of SDS, which suggests that α-synuclein has an intrinsic propensity for adopting multiple α-helical structures even in the absence of micelle or membrane binding, a feature that may have implications for its biological activity and toxicity. Additionally, we discuss the relation between α-synuclein three-state folding and its aggregation, within the context of isothermal titration calorimetry and transmission electron microscopy measurements of SDS-initiated oligomer formation.

α-Synuclein is a small (14 kDa, 140 amino acids), highly acidic, intrinsically unstructured protein that is expressed predominantly in the human brain and concentrated in presynaptic nerve terminals (*1*−*3*). The protein has been substantially implicated in the pathology of Parkinson's disease, the second most common neurodegenerative disorder, affecting approximately 1% of the population by the age of 65 and 4−5% by age 85 (*4*−*9*). The protein has also been shown to play a major role in the pathology of dementia with Lewy bodies and multiple-system atrophy (*10*−*13*). In addition, the hydrophobic central region of α-synuclein (residues 61−95), also known as the "non-Aβ component of Alzheimer's disease amyloid" (NAC),[1] is a minor protein component of neuritic plaque amyloids in Alzheimer's disease, the most common neurodegenerative disorder (*9*, *14*). Several potential physiological roles have been attributed to α-synuclein. Due to its presence in presynaptic nerve terminals, its function was thought to be in neurotransmitter release and vesicle recycling (*15*−*18*). This hypothesis is supported by recent work suggesting a molecular chaperone role for α-synuclein in maintenance of SNARE complexes (*19*). Neuroprotective functions via dopamine regulation and against glutamate-induced excitotoxicity have also been attributed to the protein (*20*, *21*). Other recent work provides strong evidence of the inhibition of ER−Golgi vesicular transport by α-synuclein being a major determinant of α-synuclein toxicity (*22*).

The α-synuclein sequence can be divided into three regions, an N-terminal region (residues 1−60) containing seven 11-amino acid imperfect repeats, a central hydrophobic region (residues 61−95; NAC), and a highly negatively charged, proline-rich, and predominantly unstructured C-terminal region (residues 96−140) (*23*, *24*). The N-terminal region imperfect repeats encode amphipathic helices that are involved in membrane binding, likely playing a key role in binding of α-synuclein to synaptic vesicles (*24*−*26*). The core region of the amyloid structure (roughly amino acids 38−95) has been shown to contain the entire NAC region, as well as a part of the N-terminal region (*27*−*29*). Finally, although considered predominantly unstructured, the C-terminal region has been suggested to play a regulatory role in protecting the NAC region from aggregation (*26*, *30*−*33*) as well as potentially in anchoring binding partners to lipid vesicles (*31*). The amino acid distribution of α-synuclein matches the general requirements for a natively unfolded protein (i.e., low hydrophobicity and high net charge) (*34*), and the protein is indeed unstructured under dilute buffer conditions (*3*).

In vitro, α-synuclein forms characteristic fibrils that have staining properties and morphology similar to those extracted from disease-affected brain (*35*−*37*). The kinetics of α-sy-

[†] This work was supported by a National Institute of General Medical Sciences grant (GM066833) from the National Institutes of Health (to A.A.D.). A.C.M.F. is a recipient of a Ruth L. Kirschstein National Research Service Award postdoctoral fellowship from the National Institute of Neurological Disorders and Stroke, National Institutes of Health.

* To whom correspondence should be addressed. Telephone: (858) 784-9192. Fax: (858) 784-9067. E-mail: deniz@scripps.edu.

[1] Abbreviations: CD, circular dichroism; CMC, critical micelle concentration; ITC, isothermal titration calorimetry; NAC, non-Aβ component of Alzheimer's disease amyloid; NLS, nonlinear least squares; SDS, sodium dodecyl sulfate; TEM, transmission electron microscopy.

10.1021/bi602461y CCC: $37.00
Published on Web 03/23/2007

nuclein fibrillation are consistent with a nucleation-dependent mechanism (*37*, *38*), implying a role for a critical intermediate in the early stages of the aggregation process (*39*). In principle, any species in the α-synuclein fibrillation pathway is a valid target for the inhibition or reversal of fibril formation. In particular, protein species or conformational states that have predominant roles in the early stages of fibrillation or misfolding may be attractive targets for therapeutic intervention aimed at disease prevention or arrested disease progression. In this context, although an early intermediate has been suggested in the pathway of fibril formation (*39*, *40*), to date, there is limited understanding of the thermodynamic and structural behavior of this intermediate. To gain a better understanding of α-synuclein conformational states and their properties, we carried out a detailed thermodynamic characterization of α-synuclein folding in the presence of sodium dodecyl sulfate (SDS), a well-characterized phospholipid mimetic (*41*−*45*). Circular dichroism (CD) measurements of α-synuclein folding, in conjunction with isothermal titration calorimetry (ITC) and transmission electron microscopy (TEM) measurements of α-synuclein aggregation, are presented here.

MATERIALS AND METHODS

Chemicals. Ultrapure SDS was purchased from USB Corp. (lot 115177). All other chemicals were either analytical or reagent grade.

Protein Expression and Purification. The plasmid construct for α-synuclein was kindly provided by R. L. Nussbaum (National Institutes of Health, Bethesda, MD). The construct is a modification of pET-41a (Novagen, EMD Biosciences, Inc.) and has been described previously (*46*). The construct was checked for the correct insert by sequencing (Center for Nucleic Acid Research, The Scripps Research Institute) and transformed into *Escherichia coli* T7 expression strain BL21(DE3). Protein purification was carried out on the basis of the description of Jakes et al. (*2*) with modifications as described below. Transformed cells were grown in LB medium at 37 °C with shaking until the OD_{600} reached ∼0.5−0.7 (2−2.5 h) and then induced by addition of IPTG (final concentration of 1 mM). Cells were grown for an additional ∼3 h, harvested and collected via centrifugation, resuspended in buffer [i.e., 50 mM Tris-HCl (pH 7.5)] with 50 mM NaCl and 1 mM EDTA, frozen and thawed three times by alternating between −80 °C and room temperature, sonicated, and then centrifuged to remove cell debris. The crude lysate was incubated at 80 °C for 10 min and centrifuged to separate the precipitate. The supernatant was further purified using a Q-Sepharose (Amersham Biosciences) column with a stepwise gradient of 50, 150, and 300 mM NaCl (using buffer without EDTA). The majority of α-synuclein elutes at 300 mM NaCl. Fractions containing α-synuclein were then mixed at a 1:5 (v/v) ratio with a 50 mM sodium acetate solution and combined with SP-Sepharose (Amersham Biosciences) beads (using ∼0.5 mL of hydrated resin/L of culture). The mixture was adjusted to pH 5.7, incubated at 4 °C with stirring for a minimum of 1 h, and filtered to separate the beads from the supernatant. The supernatant was then mixed with Q-Sepharose beads (0.5 mL of hydrated resin/L of culture), adjusted to pH 4.4, incubated at 4 °C with stirring for a minimum of 1 h, and filtered again to collect the supernatant. The final purification was performed using reverse phase chromatography, employing a C4 column. The purity of the final product was verified by SDS−PAGE. The molecular weight was verified using matrix-assisted laser desorption ionization time-of-flight mass spectrometry (Scripps Center for Mass Spectrometry).

Protein concentrations were determined spectrophotometrically using the Edelhoch method, detecting protein UV absorbance in 6.0 M guanidine hydrochloride and 20 mM phosphate (pH 6.5). An extinction coefficient of 5120 M^{-1} cm^{-1} was used for measurements carried out at 280 nm (*47*−*49*).

Detection of SDS Micelle Formation by Isothermal Titration Calorimetry. SDS micelle formation in buffer solution (i.e., 0.2 M NaCl, 10 mM sodium acetate, 10 mM NaH_2PO_4, and 10 mM glycine) at 25.0 ± 0.2 °C was detected via ITC using a MicroCal VP-ITC microcalorimeter (*50*). Heats of mixing between 50 mM SDS in buffer solution and buffer solution alone were determined by performing, at 2 min intervals, 59 stepwise 5 μL injections of the SDS solution (pH 7.00 ± 0.05) into the 1.435 mL calorimeter cell containing SDS-free buffer solution (pH 7.00 ± 0.05). Heats of mixing data were then analyzed assuming a two-state monomer to micelle transition accompanied by enthalpy changes that are proportional to changes in SDS monomer and micelle populations. Specifically, fractions of SDS molecules in monomeric form ($f_{Monomer}$) at different detergent concentrations were calculated using the equation

$$f_{Monomer} = (y_{Micelle} - y_i)/(y_{Micelle} - y_{Monomer}) \quad (1)$$

where y_i is the observed enthalpy change at a specific SDS molar concentration i (expressed in pSDS or $-\log[i]$) and $y_{Monomer}$ and $y_{Micelle}$ represent the pre- and postmicelle formation baselines, respectively, which are sufficiently described as linear functions of pSDS.

Far-UV CD Spectroscopy. Protein secondary structure perturbations induced by SDS, temperature, and pH were monitored using an Aviv model 62DS/202SF CD spectrometer equipped with a Peltier automated temperature control unit.

Measured CD signals at specific wavelengths were expressed as mean residue ellipticity $[\theta]_\lambda$ (degrees square centimeters per decimole), calculated using the expression

$$[\theta]_\lambda \equiv \theta_\lambda/(10Cnl) \quad (2)$$

where θ_λ is the observed ellipticity in millidegrees at wavelength λ, C is the molar protein concentration, n is the number of amino acid residues per protein molecule, and l is the pathlength in centimeters.

Wavelength (and temperature) scans were carried out using a bandwidth of 1 nm, a minimum averaging time of 5 s, and a 0.1 cm pathlength cuvette maintained at a specific temperature with a precision of 0.1 °C. Unless otherwise stated, experiments were performed using a protein concentration of 20 μM and thermal scans were carried out using a scan rate of ∼1.4 °C/min. All measurements were corrected for solvent contributions. Analyses of thermal unfolding data were performed via nonlinear least-squares (NLS) fitting to a three-state model (described below) using Origin (OriginLab).

Analysis of α-Synuclein Multistate Thermal Unfolding Transitions. Protein folding−unfolding data involving multiple conformational states, as described by the reaction S1 ↔ S2 ↔ ⋯ ↔ S*n*, may be graphically analyzed using the equation

$$\epsilon = \epsilon_{S1} + \sum_{i=2}^{n} f_{Si}(\epsilon_{Si} - \epsilon_{S1}) \quad (3)$$

where ϵ represents any observable able to distinguish the n different states and is proportional to the concentration of protein species in solution, S*i* denotes any of the unique states (i.e., S1, S2, ..., or S*n*), f_{Si} corresponds to the fraction of the total protein population that exists as state S*i*, and ϵ_{Si} represents the observable exhibited by S*i*.

Each S*i* ↔ S*i*+1 equilibrium can be described by an equilibrium constant K_i as defined by

$$K_i \equiv \frac{[Si+1]}{[Si]} \quad (4)$$

K_i relates to the Gibbs free energy difference (ΔGi) between states S*i*+1 and S*i*, as expressed by the equation

$$K_i = e^{-(\Delta Gi/RT)} \quad (5)$$

where R is the ideal gas constant and T is the absolute temperature. A partition function Q is defined by

$$Q \equiv 1 + K_1 + K_1K_2 + ... + K_1K_2\cdots K_{n-1} \quad (6)$$

The fraction of the total protein population that exists as S1 is given by $1/Q$, while that for each other protein species S*i* (i.e., $i \neq 1$) is given by the equation

$$f_{Si} = \frac{\prod_{j=1}^{i-1} K_j}{Q} \quad (7)$$

α-Synuclein thermal denaturation experiments were performed by monitoring protein ellipticity under different solution conditions, varying pH and SDS concentration. Thermal scan data were analyzed by applying eq 3 to a three-state equilibrium composed of folded (F), intermediately folded (I), and unfolded (U) states, as described by the reaction F ↔ I ↔ U. Specifically, unfolding transition data were fit to the equation

$$\epsilon = \epsilon_F + f_I(\epsilon_I - \epsilon_F) + f_U(\epsilon_U - \epsilon_F) \quad (8)$$

ϵ_F, ϵ_I, and ϵ_U are the transition baselines for F, I, and U, respectively, and are sufficiently described as linear functions of temperature. f_I and f_U, which represent the fractional populations of I and U, are given by K_1/Q and K_1K_2/Q, respectively (eq 7). $Q = 1 + K_1 + K_1K_2$, where K_1 and K_2 are $e^{-(\Delta G1)/(RT)}$ and $e^{-(\Delta G2)/(RT)}$, respectively (eqs 5 and 6). The functional dependence of $\Delta G1$ or $\Delta G2$ (i.e., ΔGi, where $i = 1$ or 2) on the absolute temperature T is given by the Gibbs−Helmholtz relationship:

$$\Delta Gi = \Delta Hi\left(1 - \frac{T}{T_{mi}}\right) + \Delta C_{pi}\left(T - T_{mi} - T\ln\frac{T}{T_{mi}}\right) \quad (9)$$

T_{mi} (T_m^{F-I} or T_m^{I-U}) is the thermal transition midpoint for the transition S*i* → S*i*+1, i.e., F → I or I → U. ΔHi (ΔH^{F-I} or ΔH^{I-U}) is the transition enthalpy change at T_{mi}. ΔC_{pi} (ΔC_p^{F-I} or ΔC_p^{I-U}) is the difference in heat capacity between S*i*+1 and S*i*, i.e., I and F, or U and I.

Initiation of α-Synuclein Aggregation by SDS As Detected by Isothermal Titration Calorimetry. SDS-induced aggregation of α-synuclein in buffer [i.e., 0.2 M NaCl, 10 mM sodium acetate, 10 mM NaH_2PO_4, and 10 mM glycine (pH 2.50 ± 0.05)] was detected using ITC (employing the same Microcal VP-ITC instrument mentioned above). Following an initial time delay of 120 s, protein aggregation was initiated by performing single 200 μL injections of buffered SDS solutions (8.17 mM SDS) into the 1.435 mL calorimeter cell containing buffered protein solution (22.8 μM α-synuclein), pre-equilibrated at the temperature of interest (±0.2 °C). The time duration for the SDS injections is 250 s. The final protein and SDS concentrations in the cell are 20 μM and 1 mM, respectively. To measure SDS heats of dilution, similar experiments as described above were performed, injecting buffered SDS solutions against buffer without protein. Heats of aggregation were then calculated as the difference between the measured heats in the aggregation and the dilution experiments. Data analyses were conducted using Microcal Origin (Microcal Software, Inc.).

Transmission Electron Microscopy. Protein fibrils and aggregates were prepared by either (i) incubating 20 μM α-synuclein in 0.2 M NaCl, 10 mM sodium acetate, 10 mM NaH_2PO_4, and 10 mM glycine (pH ∼2.5) at 80 °C for 2 h and then at room temperature for 1 month or (ii) incubating 20 μM α-synuclein in 1 mM SDS, 0.2 M NaCl, 10 mM sodium acetate, 10 mM NaH_2PO_4, and 10 mM glycine (pH ∼2.5) at room temperature for 1 day or 1 month. For visualization by TEM, 4 μL of protein samples was applied to glow-discharged parlodion-coated copper grids. After adsorption was permitted for 3 min, grids were washed with deionized distilled water and then negatively stained with 2% (w/v) uranyl acetate. TEM images were collected at 80 kV on a Philips CM100 electron microscope (FEI, Hillsboro, OR) and documented using Kodak SO163 EM film. Negatives were scanned at 600 lines per inch using a Fuji FineScan 2750 device and converted to TIF format for subsequent handling in Photoshop (Adobe Systems, San Jose, CA).

RESULTS

SDS-Induced α-Synuclein Folding and Unfolding. Effects of SDS on α-synuclein secondary structure were investigated using far-UV CD spectroscopy, monitoring protein ellipticity over a broad range of SDS concentrations (0−400 mM). Figure 1 presents isothermal titration data collected at 25 °C and pH 7.0. Panels A and B show spectral data collected at 0−2 and 3−400 mM SDS, respectively. At dilute SDS concentrations (0−0.2 mM), α-synuclein exhibits "random coil" CD spectra. At higher concentrations (>0.2 mM), α-synuclein is induced to adopt structural conformations that are, on the basis of the CD spectral profiles, rich in α-helix. Figure 1C shows mean residue ellipticities at two specific wavelengths (222 and 198 nm) plotted against SDS concentration, illustrating the complex dependence of α-synuclein structural properties on SDS.

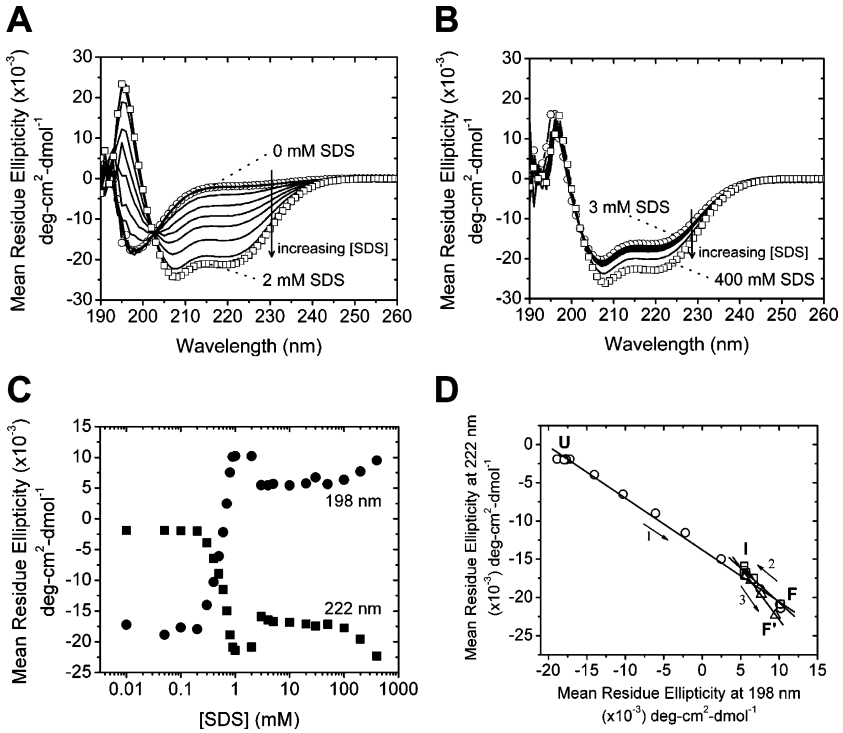

FIGURE 1: SDS-induced structural changes in α-synuclein monitored by far-UV CD spectroscopy. Wavelength scans were performed at 0.2 M NaCl, 10 mM sodium acetate, 10 mM NaH_2PO_4, and 10 mM glycine at pH 7.00 ± 0.05 and 25.0 ± 0.1 °C in the presence of varying SDS concentrations. Presented in panel A are the CD spectral data from solutions containing 0 mM SDS (○), 2.0 mM SDS (□), and intermediate SDS concentrations, i.e., 0.01, 0.05, 0.1, 0.2, 0.3, 0.4, 0.5, 0.6, 0.7, 0.8, 0.9, and 1.0 mM (—). Shown in panel B are data from solutions containing 3.0 mM SDS (○), 400 mM SDS (□), and intermediate SDS concentrations, i.e., 4.0, 5.0, 10, 20, 30, 50, 100, and 200 mM (—). CD signals at two specific wavelengths [222 (■) and 198 nm (●)] are plotted against SDS concentration in panel C. Shown in panel D are the spectral intensities at 222 nm plotted against the intensities at 198 nm. U, I, F, and F′ correspond to the different protein states. Arrows indicate the direction in which the SDS concentration is increasing.

Initial additions of SDS (≤0.2 mM) result in minimal changes in protein secondary structure. Further increases in SDS concentration from ~0.2 to 1.0 mM result in the induction of α-helical structure. From 2 to 3 mM SDS, the protein abruptly undergoes partial unfolding. From 3 to 100 mM SDS, protein secondary structure remains practically unperturbed. Finally, at concentrations greater than 100 mM, the protein is again induced to form a more α-helical structure. Titration data at the two wavelengths are in excellent agreement.

Differential α-Synuclein Interaction with Monomer and Micelle Forms of SDS. To distinguish between effects of monomeric and micellar SDS on α-synuclein, ITC was employed to characterize the detergent monomer to micelle transition under the same solution conditions used for studying the protein. Figure S1 of the Supporting Information presents the ITC data and demonstrates that micelle formation is negligible at pSDS 3 (1 mM SDS) and lower SDS concentrations (higher pSDS). Within the small effects on the SDS critical micelle concentration (CMC) of the additional buffer components (i.e., 10 mM sodium acetate, 10 mM NaH_2PO_4, and 10 mM glycine), this observation is consistent with the reported CMC of SDS in 0.2 M NaCl at 25 °C, i.e., 0.92 mM (*51*). The presence of 20 μM protein in solution does not significantly affect and decrease the SDS CMC, as evidenced by our observation that varying protein concentrations (5, 10, and 20 μM) give rise to very similar protein thermal unfolding behavior in 1 mM SDS (Figure S2 of the Supporting Information). Thus, all effects of SDS on α-synuclein structure at SDS concentrations lower than 1 mM may be attributed primarily to the monomeric form of the detergent. With that, interpretation of the CD data presented in Figure 1C is straightforward. At SDS concentrations of <1 mM, monomeric SDS molecules interact with α-synuclein and induce structure formation in a highly cooperative fashion, probably due to specific binding. As a significant population of SDS micelles is formed (at 2−3 mM SDS), the protein undergoes partial unfolding induced by binding of α-synuclein to the micelles. The ability of α-synuclein to bind SDS micelles has also been demonstrated previously (*44*, *45*). In the SDS concentration range of 3−100 mM, micelle properties presumably remain relatively constant, and thus, the detergent-bound protein is also structurally unperturbed. At extremely high SDS concentrations (200−400 mM), SDS micelle properties are significantly different from those present in more dilute detergent concentrations (e.g., higher aggregation number and lower radius of curvature) (*52*), therefore allowing the bound protein to adopt another conformation that has higher α-helical content. Employing the phase diagram method of Kuznetsova et al. (*53*), we plotted the spectral intensities at 222 nm as a function of the CD intensities at 198 nm (Figure 1D). Consistent with Figure 1C, three all-or-none transitions are clearly resolved, involving three to four structurally unique protein states (i.e., U, I, F, and F′, where U is the intrinsically unstructured state present under dilute SDS conditions, I is an intermediately folded state, and F and F′ are the most folded states). F mainly exists at pre-CMC SDS concentrations, whereas F′ is populated at extremely high SDS concentrations in which SDS micelles

adopt elongated cylindrical shapes (*52*). On the basis of their near-identical CD intensities at 222 and 198 nm, F and F′ are most likely structurally very similar.

Multistate Thermal Unfolding of α-Synuclein Folded Using SDS. To characterize the thermal folding−unfolding behavior of α-synuclein, CD wavelength scans at different temperatures (Figure 2A) and CD thermal scans at a constant wavelength (Figure 2B) were carried out in 1 mM SDS (pH 7.0), where the protein is able to adopt a stable structure and SDS molecules are predominantly in a monomeric form. Figure 2A presents α-synuclein CD spectra over a wide range of temperatures (0−100 °C, every 5 °C), in the presence of 1 mM SDS. At the lower temperatures (0−25 °C), α-synuclein assumes a conformation that is rich in α-helix. A gradual increase in temperature results in a concomitant loss of structure, eventually producing a more random coil-like conformation at the higher temperatures (90−100 °C). The 222 nm readings of the spectra were plotted as a function of temperature (effective scan rate of 0.4 °C/min) and presented in Figure 2B. Also shown in Figure 2B are thermal scan data (scan rate of 1.3 °C/min) collected using fresh and reheated samples. The three sets of data show excellent agreement, demonstrating that the protein unfolding reaction is reversible and that the thermal denaturation experiments were most likely performed under equilibrium conditions. More importantly, it is evident from the thermal scan data that α-synuclein thermal unfolding involves transitions between multiple states. A three-state model (described in Materials and Methods) was the minimal model that could describe the data, which is consistent with the two all-or-none transitions clearly resolved in the phase diagram presented in Figure 2C. To model the unfolded state (U), a thermal scan of the protein at 0 mM SDS, where it is intrinsically unfolded, was also performed. The U baseline slope and intercept parameters for the 1 mM SDS data were then fixed to coincide with the linear fit of the 0 mM SDS data (presented in Figure 2B). Baseline parameters representing the state with the most secondary structure (F) were floated. Floating the baseline slope parameter for the state with an intermediate amount of secondary structure (I) resulted in, within experimental error limits, the same slope that was observed in other measurements (e.g., 10 mM SDS data, which are also presented in Figure 2B). The I baseline slope parameter was therefore fixed and is identical to that of the least-squares line best fit to the 10 mM SDS data. Treatment of baseline parameters as described above is validated by the fact that pH perturbations that lead to more defined baselines show consistency (Figure 5).

To test whether protein oligomers (that thermally unfold reversibly and reproducibly) are involved in α-synuclein thermal unfolding transitions, 1.3 °C/min thermal scans of the protein were also performed in the presence of 1 mM SDS at pH 7.0 using protein concentrations of 10 and 5 μM (Figure S2). (Unless it is specifically stated otherwise, all experiments reported here were performed using 20 μM protein.) NLS fitting of the 20, 10, and 5 μM α-synuclein thermal scan data to the three-state model shows that all data can be described by the same thermal unfolding thermodynamic parameters, which suggests that the protein is monomeric or that the U state has the same degree of oligomerization as the F and I states. The thermally induced U state of α-synuclein in the presence of SDS exhibits random coil

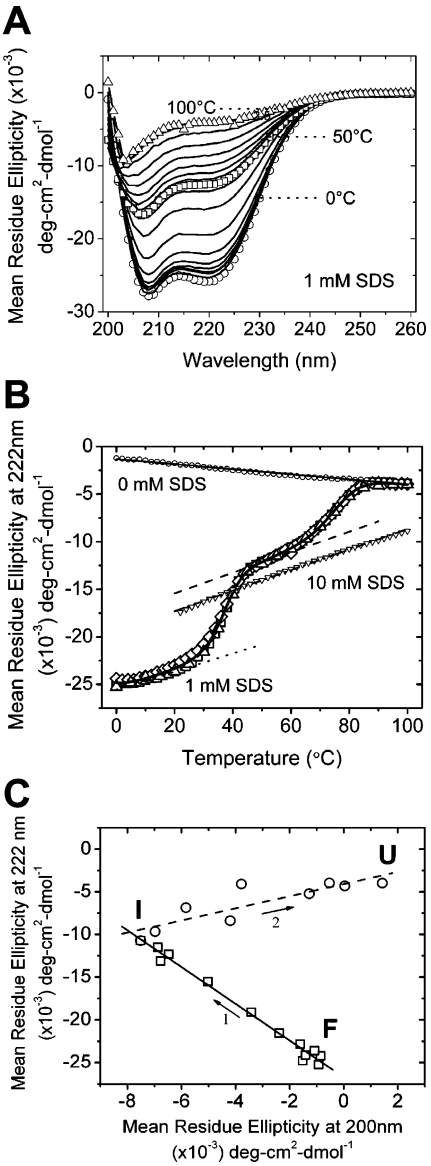

FIGURE 2: Three-state temperature-induced unfolding of α-synuclein folded using SDS. Thermal unfolding of α-synuclein was monitored at 0.2 M NaCl, 10 mM sodium acetate, 10 mM NaH_2PO_4, and 10 mM glycine at pH 7.00 ± 0.05 in the presence of 1 mM SDS. Presented in panel A are protein far-UV CD spectra collected (using a single protein preparation) at different temperatures (i.e., 0−100 °C, at 5 °C intervals). A constant wavelength slice at 222 nm of the data presented in panel A is shown in panel B [(△) effective scan rate of 0.4 °C/min]. Data from thermal scans (scan rate of 1.3 °C/min, 0−100 °C at 2 °C intervals) of the same sample used in panel A and of another fresh sample are also shown in panel B: ◇ and □, respectively. Also shown in panel B are thermal scan data at 0 (○) and 10 mM SDS (▽). The solid curve represents the nonlinear least-squares (NLS) best fit of the combined 1 mM SDS data to the multistate unfolding model described in Materials and Methods. The dotted, dashed, and solid straight lines represent the F, I, and U baselines, respectively. The U baseline slope and intercept parameters were fixed to coincide with the 0 mM SDS data. The I baseline slope parameter was fixed and is identical to that of the least-squares line best fit (dotted and dashed) to the 10 mM SDS data. Shown in panel C are the spectral intensities at 222 nm plotted against the intensities at 198 nm for the thermal denaturation data presented in panel A. Arrows indicate the direction in which the SDS concentration is increasing.

CD spectra (Figure 2A), and a random coil-like protein is most likely monomeric. In addition, the three-state model used for data analyses assumes monomeric protein states and

Table 1: SDS Concentration Dependence of Thermodynamic Parameters for the Three-State Temperature-Induced Unfolding of α-Synuclein[a]

[SDS] (mM)	T_m^{F-I} (°C)	ΔH^{F-I} (kcal/mol)	T_m^{I-U} (°C)	ΔH^{I-U} (kcal/mol)
0.5[b]	nd[d]	nd[d]	42.9 ± 6.4	8.9 ± 2.2
0.6[b]	nd[d]	nd[d]	60.1 ± 2.5	17.7 ± 1.8
0.7[b]	30.7 ± 0.3	43.8 ± 1.8	68.2 ± 0.7	27.1 ± 1.7
0.8[b]	33.1 ± 0.2	47.5 ± 1.9	69.8 ± 0.4	34.9 ± 1.8
1.0[b]	36.3 ± 0.2	58.9 ± 2.0	75.9 ± 0.2	50.9 ± 2.2
1.5[c]	43.9 ± 0.3	63.5 ± 0.7	86.1 ± 0.3	56.2 ± 3.2
2.0[c]	37.7 ± 0.3	57.3 ± 1.2	93.0 ± 0.4	52.0 ± 3.3
2.5[c]	23.7 ± 0.7	46.7 ± 6.4	102.0 ± 0.9	51.6 ± 6.1
3.0[c]	nd[d]	nd[d]	106.6 ± 2.2	50.6 ± 9.6
3.5[c]	nd[d]	nd[d]	110.0 ± 4.5	52.8 ± 15.9

[a] Errors reported are estimated standard errors (Origin). [b] Monomeric SDS regime; NLS fitting performed simultaneously, assuming temperature- and SDS concentration-independent ΔC_p^{F-I} (2.5 ± 0.1 kcal mol^{-1} °C^{-1}) and ΔC_p^{I-U} (0.34 ± 0.02 kcal mol^{-1} °C^{-1}). [c] NLS fitting performed simultaneously, fixing ΔC_p^{F-I} (2.5 kcal mol^{-1} °C^{-1}) and ΔC_p^{I-U} (0.34 kcal mol^{-1} °C^{-1}). [d] Not determined.

Table 2: pH Dependence of Thermodynamic Parameters for the Three-State Thermal Unfolding of α-Synuclein[a]

pH	T_m^{F-I} (°C)	ΔH^{F-I} (kcal/mol)	T_m^{I-U} (°C)	ΔH^{I-U} (kcal/mol)
5.0	48.1 ± 0.1	64.5 ± 1.6	nd[b]	nd[b]
5.4	45.3 ± 0.2	60.2 ± 1.5	99.5 ± 0.6	58.7 ± 6.5
5.9	41.9 ± 0.2	56.0 ± 1.4	93.2 ± 0.4	64.5 ± 5.0
7.0	36.6 ± 0.2	51.4 ± 1.4	76.2 ± 0.2	53.8 ± 2.6
8.4	34.3 ± 0.2	48.0 ± 1.4	75.1 ± 0.2	52.2 ± 2.3
9.5	32.7 ± 0.2	43.3 ± 1.3	73.9 ± 0.2	48.7 ± 2.1
11.1	19.5 ± 0.2	54.5 ± 3.9	57.2 ± 0.3	32.1 ± 1.3
11.8	nd[b]	nd[b]	48.4 ± 1.4	22.1 ± 2.3
12.5	nd[b]	nd[b]	44.2 ± 4.6	16.5 ± 4.9
13.0	nd[b]	nd[b]	47.6 ± 1.3	17.8 ± 1.5

[a] Errors reported are estimated standard errors (Origin); NLS fitting performed simultaneously, assuming temperature- and SDS concentration-independent ΔC_p^{F-I} (2.2 ± 0.1 kcal mol^{-1} °C^{-1}) and ΔC_p^{I-U} (0.65 ± 0.03 kcal mol^{-1} °C^{-1}). [b] Not determined.

is demonstrated here to be consistent with data collected over a wide range of temperatures, SDS concentrations, and pH conditions. Finally, ΔC_p values acquired for the thermal transitions of α-synuclein (and reported in Tables 1 and 2) are appropriate only for a small protein (*54*). For these reasons, the involvement of oligomeric protein states in the thermal unfolding transitions investigated here is highly unlikely.

SDS Concentration Dependence of α*-Synuclein Thermal Unfolding.* Changes in α-synuclein thermal denaturation properties at pH 7.0 in response to variations in SDS concentration were also investigated. Panels A and B of Figure 3 present CD thermal scan data recorded at two different SDS concentration regimes, i.e., pre- and post-CMC, respectively. Data were analyzed using the same multistate model mentioned above. Evident from the quality of the NLS fits of the data in panels A and B of Figure 3, the model works in describing α-synuclein−SDS monomer and α-synuclein−SDS micelle interactions. At low SDS concentrations (e.g., 0−0.6 mM), cold denaturation is observed even at temperatures above 0 °C. At higher SDS concentrations, cold denaturation is predicted to occur at much lower temperatures (see the inset of Figure 3A). α-Synuclein is, as expected, unfolded at all temperatures at dilute SDS concentrations. The thermal unfolding thermodynamic parameters derived from the data analyses performed are

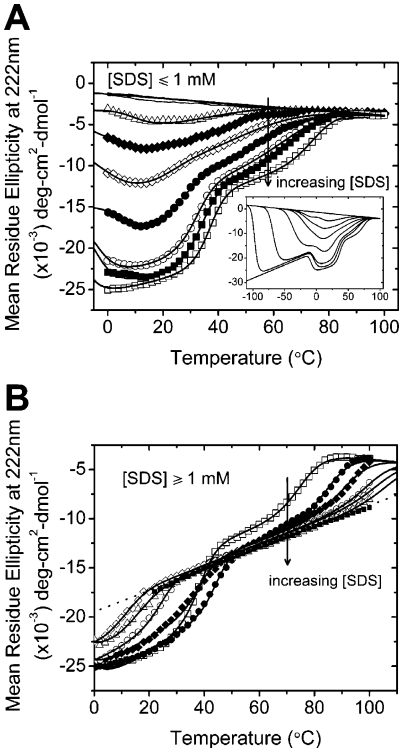

FIGURE 3: SDS concentration dependence of α-synuclein three-state thermal unfolding. Thermal scans were carried out at 0.2 M NaCl, 10 mM sodium acetate, 10 mM NaH_2PO_4, and 10 mM glycine at pH 7.00 ± 0.05 in the presence of varying SDS concentrations. Shown in panel A are thermal denaturation data under conditions where SDS molecules are predominantly monomeric, i.e., 0, 0.05, 0.1, and 0.2 mM SDS (−) and 0.3 (△), 0.4 (◆), 0.5 (◇), 0.6 (●), 0.7 (○), 0.8 (■), and 1.0 mM SDS (□). Presented in panel B are denaturation data in 1.0 (□), 1.5 (●), 2.0 (◆), 2.5 (○), 3.0 (◇), 3.5 (△), and 10 mM SDS (■). Solid curves in panels A and B represent the three-state unfolding model NLS best fits of the data, with baseline parameters treated in the same manner as that described in the legend of Figure 2. Straight lines in panels A and B correspond to the least-squares best fit lines to the 0 and 10 mM SDS data, respectively. The NLS best fit curves in panel A are also shown over a broader temperature range to highlight protein cold denaturation (inset).

summarized in Table 1, with the transition midpoints (T_m^{F-I} and T_m^{I-U}) plotted against pSDS in Figure 4.

α-Synuclein SDS−Temperature Protein Phase Diagram. The protein phase diagram method reported by Rösgen and Hinz (*55*) and Ferreon et al. (*56*) was employed in analyzing the data presented in Figure 4. Results of the phase diagram analyses showed that the transitions from U to I, I to F, and U_m to I_m each involve the binding of five SDS molecules. In contrast, the transition from I_m to F (in the 20−45 °C region), on average, is characterized by a loss of ∼12 SDS molecules. From the SDS−temperature protein phase diagram, it is apparent that F exists only in a very narrow range of SDS concentrations and temperatures. Each of the I and U ensembles may be divided into two sub-ensembles, micelle-bound and unbound, although a clear distinction between the sub-ensembles is difficult to establish experimentally. Thus, to approximate the 50% phase separation lines between the micelle-bound and unbound states, the midpoint of SDS micelle formation in buffer was used. Comparing the I baselines derived from the three-state model NLS best fit curve of the 1 mM SDS thermal scan data and the least-squares best fit line of the 10 mM SDS data (both

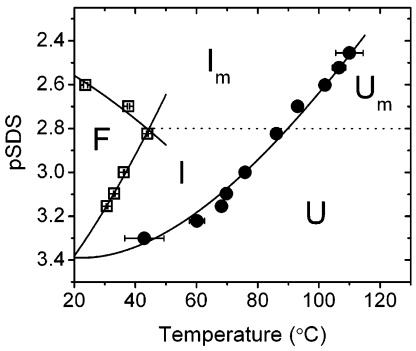

FIGURE 4: SDS−temperature phase diagram of α-synuclein. Transition midpoints of F → I (□) and I → U (●) transitions are plotted against pSDS (i.e., −log[SDS]). Solid curves represent the 50% phase separation lines. The dotted line denotes the midpoint of SDS micelle formation in buffer at 25 °C (i.e., pCMC = pSDS 2.8; see Figure S1). F, I, and U, and I_m and U_m, correspond to the different protein states that exist under monomeric and micellar SDS conditions, respectively. Phase separation lines were determined by NLS fitting using the equation $pSDS_{mid} = (npk_{ref} - \log K)/n$, where $K = \exp[-(\Delta G/RT)]$, $\Delta G = \Delta H^{ref}(1 - T/T_m^{ref}) + \Delta C_p^{ref}(T - T_m^{ref} - T \ln T/T_m^{ref})$, $pSDS_{mid}$ is the ligand binding transition midpoint at the absolute temperature T, n is the change in the number of SDS monomers bound to the protein, T_m^{ref} is an arbitrary reference temperature (chosen to be at a known thermal transition midpoint), and pk_{ref}, ΔH^{ref}, and ΔC_p^{ref} are the $pSDS_{mid}$, enthalpy change, and heat capacity change at T_m^{ref}, respectively. ΔC_p^{ref} is determined from the slope of a ΔH vs T_m plot (data reported in Table 1). n and pk_{ref} are NLS fitting parameters.

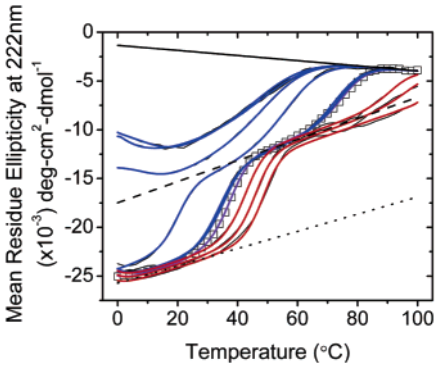

FIGURE 5: pH dependence of α-synuclein three-state thermal unfolding. Thermal scans were performed at 1 mM SDS, 0.2 M NaCl, 10 mM sodium acetate, 10 mM NaH_2PO_4, and 10 mM glycine, employing different pH conditions, i.e., pH 7.0 (□, violet NLS best fit curve), pH 5.9, 5.4, and 5.0 (black lines, left to right from pH 7.0 data; red NLS best fit curves), and pH 8.4, 9.5, 11.1, 11.8, 12.5, and 13.0 (black lines, right to left from pH 7.0 data; blue NLS best fit curves). Dotted, dashed, and solid straight lines denote the F, I, and U baselines, respectively.

presented in Figure 2B), we find that the micelle-bound I state is slightly more structured than the unbound state at all the temperatures that were investigated. Three-state analysis of the isothermal titration data presented in Figure 1C (using only the data points derived under conditions where SDS is primarily monomeric) shows consistency with the results of the protein phase diagram analyses, within experimental error limits (see Figure S3 of the Supporting Information).

pH Dependence of α-Synuclein Three-State Unfolding. To further characterize the multistate folding and unfolding behavior of α-synuclein, CD thermal scans were also performed in the presence of 1 mM SDS at various pH conditions (pH 5−13), with the data presented in Figure 5. (Note that below pH 5, all thermal unfolding transitions become irreversible due to protein aggregation.) Data analyses were performed using the same three-state model mentioned above, with a summary of the fitted thermal unfolding thermodynamic parameters presented in Table 2. A clear trend is that both the transition midpoints T_m^{F-I} and T_m^{I-U} increase with a decrease in pH; i.e., acidic conditions favor partial and complete structure formation at 1 mM SDS. Under alkaline conditions, F becomes highly disfavored and thermal unfolding transitions essentially become two-state. Furthermore, I is destabilized relative to U under alkaline conditions, which is manifested in a decreased T_m^{I-U}. The destabilization is, however, not sufficient for base denaturation at room temperature even at a pH as high as 13.

α-Synuclein Aggregation Initiated by SDS. A dilute concentration of α-synuclein (20 μM) at pH 2.5 is stably soluble for hours even at elevated temperatures (e.g., 80 °C), as evidenced by a flat baseline when the sample is observed (without injection) using an isothermal titration calorimeter. Addition of SDS (final concentration of 1 mM), however, results in practically instantaneous aggregation, with clearly visible aggregates formed in solution. This SDS-initiated α-synuclein aggregation was investigated using ITC and TEM. Figure 6A shows representative ITC data collected at 37 °C and pH 2.5. ITC measurements were performed at six different temperatures, with a summary presented in Figure 6B as a plot of the apparent enthalpy change of aggregation ($\Delta H^{apparent}$) versus temperature. At all the temperatures that were studied, SDS-induced α-synuclein aggregation was found to be exothermic, with the initial aggregation process defined by a heat capacity change ($\Delta C_p^{Aggregation}$) of -5.04 ± 0.17 kcal mol^{-1} °C^{-1}.

To further characterize the detergent-induced aggregation of α-synuclein, TEM was employed for visualization of protein aggregates formed at pH 2.5 in the presence (Figure 6E,F) and absence (Figure 6C,D) of SDS. A 1 month incubation of the protein in pH 2.5 buffer without SDS (after initial incubation at 80 °C for 2 h) resulted in the formation of fibrillar aggregates (Figure 6C). Individual fibrils interact with other fibrils, forming side-to-side contacts. Gentle agitation of the fibrils by centrifugation and resuspension resulted in the formation of non-fibrillar aggregates composed of individual and "clumped" spheres of variable size (Figure 6D). A TEM image of 1-day-old protein aggregates formed in the presence of 1 mM SDS at room temperature is shown in Figure 6E. The aggregates are composed of spheres with variable size and strings of interacting spheres. An additional 1 month incubation of a sample similar to that shown in Figure 6E results in the formation of string-like aggregates with more fibril-like morphology and dimensions (Figure 6F).

DISCUSSION

Multistate Folding of α-Synuclein in the Presence of SDS. SDS is commonly known as a protein denaturing agent (*57*, *58*). It is, however, well-documented that the detergent can induce structure formation in α-synuclein (*26*, *45*, *59*), effectively mimicking phospholipids that have similar effects on the protein (*24*−*26*, *60*). In addition, both functional and toxic roles have been attributed to α-synuclein via mechanisms that require phospholipid binding (*19*, *22*). Thus,

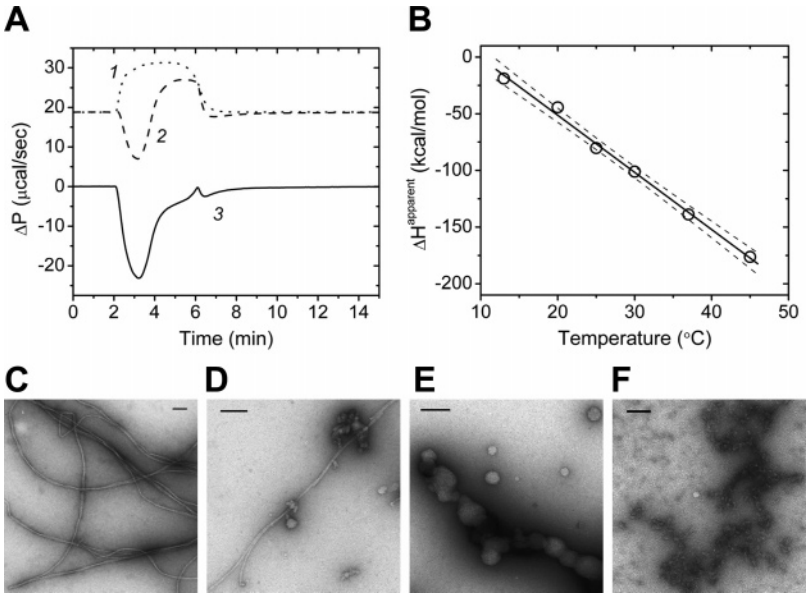

FIGURE 6: SDS-initiated α-synuclein aggregation characterized using ITC and TEM. α-Synuclein aggregation induced by SDS was investigated in 0.2 M NaCl, 10 mM sodium acetate, 10 mM NaH_2PO_4, and 10 mM glycine at pH 2.50 ± 0.05 and different temperatures (i.e., 13.0, 20.0, 25.0, 30.0, 37.0, and 45.0 °C) via ITC and at room temperature by TEM. (A) ITC data collected at 37.0 °C, where trace *1* represents heat of mixing data between SDS solution and buffer solution, trace *2* represents heat of mixing data between SDS solution and protein solution, and trace *3* is the difference between traces *2* and *1*. (B) Temperature dependence of the apparent enthalpy change of aggregation ($\Delta H^{apparent}$). From the slope of the least-squares best fit line (solid line; dashed lines represent the 0.95 confidence error bands), the apparent heat capacity change of aggregation ($\Delta C_p^{Aggregation}$) is −5.04 ± 0.17 kcal mol^{-1} °C^{-1}. (C−F) TEM images of α-synuclein fibrils and aggregates in the absence (C and D) and presence (E and F) of 1 mM SDS. Panel C presents a TEM image of α-synuclein fibrils incubated in buffer at room temperature for 1 month (after initial incubation at 80 °C for 2 h). Mechanical perturbation by centrifugation of the fibrils shown in panel C resulted in the formation of some nonfibrillar aggregates (D). Panel E shows a TEM image of 1-day-old protein aggregates induced by SDS. Panel F is similar to panel E, but with the sample incubated for 1 month. Bars are 100 nm long.

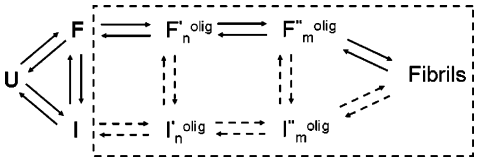

FIGURE 7: Model for α-synuclein folding and aggregation. Monomeric α-synuclein folding (left of dashed box) and possible simplified model for α-synuclein misfolding and aggregation (dashed box). U, I, and F represent the three monomeric protein states with increasing α-helical content. $F'_n{}^{olig}$, $F''_m{}^{olig}$, $I'_n{}^{olig}$, and $I''_m{}^{olig}$ represent different on- or off-pathway oligomeric states populated during fibril formation.

studies of α-synuclein conformational properties in the presence of SDS or other lipid mimetics are directly relevant for understanding the protein's physiological role.

A general three-state model describing the folding of monomeric α-synuclein emerges from our extensive thermodynamic studies performed under different SDS, temperature, and pH conditions. This model is depicted in Figure 7 (to the left of the dashed box). There are three well-defined equilibrium thermodynamic states: an unfolded state (U), a state with high degree of α-helical character (F), and another state exhibiting intermediate folding (I). Changes in solution conditions (e.g., SDS concentration, pH, and temperature) effectively shift the population of each of the F, I, and U states (Figure 4). This observation of distinct helical states under different conditions highlights the apparent intrinsic propensity of α-synuclein to adopt alternate conformational states in the presence of lipid-like molecules. It remains to be seen whether these alternate conformations are important in the synaptic or other biological functions of α-synuclein.

It is important to note that some structure is also induced in α-synuclein at increased temperatures or lowered pH [Figure 2B and Figure S4 of the Supporting Information (*39*)]. However, the level of structure induced under these conditions is minimal. Furthermore, no cooperative temperature-induced transition is observed in the absence of SDS. Therefore, the previously observed partially folded forms of α-synuclein at high temperature or acidic pH are very different from the F and I thermodynamic states that we observe in the presence of SDS. In addition, simple and fluorinated alcohols have been demonstrated to induce folding in α-synuclein (*61*). In the case of the simple alcohols (i.e., methanol, ethanol, and propanol), folding of the protein occurs over a broad range of concentrations (e.g., 10−60%, v/v) and was found to correlate with the decrease in the dielectric constant of the media. In contrast, the monomeric form of SDS induces α-synuclein folding within a very narrow range of concentrations (e.g., 0.2−1.0 mM), and SDS at concentrations below the CMC does not significantly affect the dielectric constant of the solution (*62*). Fluorinated alcohols (i.e., 2,2,2-trifluoroethanol and 1,1,1,3,3,3-hexafluoro-2-propanol) exhibited more complex behavior (*61*). A common theme for all the cosolvents (i.e., simple and fluorinated alcohols, and SDS), however, is that at relatively lower cosolvent concentrations, partially folded intermediates that enhance the protein's propensity to aggregate are populated, which suggests that α-synuclein has a strong intrinsic propensity to form such intermediates.

Possible Structures of the F and I States. Apparently conflicting reports about the structure of α-synuclein induced in the presence of lipids and lipid mimetics have appeared in the literature. Several NMR structural studies of wild-

type and mutant (A30P and A53T) α-synuclein have been carried out in the presence of SDS micelles (*26*, *43*, *44*, *63*). These NMR data are all consistent with an α-synuclein structure composed of two amphipathic helices (i.e., residues 1−41 and 45−94), separated by a short loop or a break at residues 42−44. Backbone dynamics studies also indicated flexibility in the linker region (*44*). In contrast with these NMR results, EPR analysis of several site-labeled α-synuclein mutants in small unilamellar vesicles was interpreted as evidence of an elongated helical structure devoid of significant tertiary packing (*24*). Residues 42−44 were seen to be ordered, and residue 44 was seen to be involved in membrane interaction. The apparent discrepancy in the two sets of structures has been attributed to differences in the nature of SDS micelles and small unilamellar vesicles. It has been suggested that α-synuclein binding as a single contiguous helix to high-curvature SDS micelles would result in curvature-induced strain in the protein, thereby forcing it to instead adopt a broken helix structure (*24*). Our results provide a link between the two seemingly unrelated structures and also allow the different observations to be placed within the context of a unified multistate folding model. In the regime of SDS concentrations used in the NMR structural studies (i.e., much above CMC), we observe the partially folded micelle-bound I state, which must therefore correspond to the broken helix structure observed by NMR (*44*). From Figure 2B, this micelle-bound I state is slightly more structured compared to its unbound counterpart. However, the thermal response behavior of the two forms of I state is very similar, as evidenced by the virtually identical slopes describing the temperature dependence of the mean residue ellipticities. This observation supports the idea that the micelle-bound and unbound forms of the I state have very similar structures and interactions with SDS, also consistent with the results of our protein phase diagram analyses (Figure 4). We therefore suggest that the I state observed in the absence of micelles is also a broken α-helix and that the somewhat higher average level of structure observed above CMC may be due to the greater rigidity (and hence stability) imposed on the α-helical structure in the micelle-bound state. Additionally, given its high α-helicity, we suggest that the observed F state may correspond to an elongated helix similar to that observed by EPR. A state with similarly high α-helicity is also populated at very high SDS concentrations (i.e., >200 mM; see panels B and C of Figure 1), where elongated and lower-curvature SDS micellar structures are expected (*52* and references cited therein). These observations are consistent with discontinuous features in NMR chemical shift data, which hinted at multiple α-synuclein transitions during a SDS titration (*44*). To conclude, our data indicate that SDS is capable of inducing a folded form of α-synuclein with high α-helicity and that α-synuclein can exist in multiple structural and thermodynamic forms at different SDS concentrations. This conformational plasticity may be essential for the role of α-synuclein as a molecular chaperone, facilitating the folding and refolding of SNARE complexes (*19*). Its structural transitions possibly play a role as functional switches in the rapid regulation of neurotransmitters necessary in nerve terminals.

Role of F and I States in α-Synuclein Fibrillation. Although the formation of fibrillar α-synuclein aggregates is a major pathological symptom in patients with Parkinson's disease, the structural and mechanistic basis for α-synuclein aggregation is yet to be well understood. Conditions promoting accumulation of partially unfolded protein conformations often promote protein aggregation (*64*). Furthermore, previous work on α-synuclein has also demonstrated that partial structure formation can accelerate the aggregation process (*39*, *61*). Our three-state model for α-synuclein folding in the presence of SDS, accompanied by significant increases in structure, raises the question of whether aggregation may proceed via one of the partially folded states. Our results indeed show that conditions that favor populating F (low pH, 1 mM SDS) result in very rapid aggregation. However, our EM data show that while rapid aggregation to smaller oligomeric species is accelerated by SDS, the transformation to fibrils is retarded. Interestingly, smaller aggregates with similar morphology are obtained by gentle mechanical agitation of long fibrils (Figure 6D), raising the possibility that the oligomeric aggregates observed in the presence of SDS may be kinetically trapped structural intermediates on the fibrillation pathway. In contrast with the observed accelerated aggregation at low pH, we find that conditions favoring the I state (high pH, 1 mM SDS) result in no significant aggregation. Even preformed aggregates are dissolved under alkaline conditions. These results appear to indicate that aggregation may proceed via the F state. However, given the complexities of even a highly simplified aggregation model (Figure 7), a more detailed mechanistic understanding of this process must await further experimentation.

In conclusion, we have carried out a detailed thermodynamic analysis of α-synuclein folding by SDS. We find that a minimal three-state folding model explains our data under a variety of SDS, temperature, and pH conditions. This natively unfolded protein appears dynamic, having the ability to adopt distinct structures under different conditions, features that may play important roles in its biological activity. Finally, conditions stabilizing the F state accelerate aggregation to smaller oligomers, which may either be on-pathway intermediates to fibrillation or off-pathway trapped species. While the basis for α-synuclein toxicity is still the subject of debate, a key role for oligomeric intermediates has been identified (*65*−*68*). The formation of smaller aggregates from fibrils by gentle mechanical agitation suggests that fibrils may also be fragmented to smaller and potentially toxic oligomeric species in vivo, indicating that inhibition of earlier stages of aggregation may be preferable as a therapeutic strategy against α-synuclein-related diseases. In this context, further understanding of the specific pathway leading from the natively unfolded state of monomeric α-synuclein via the F or I states to oligomeric aggregates or fibrils may provide insights into the design of drugs inhibiting specific early steps in this complex process.

ACKNOWLEDGMENT

We are grateful to Dr. Robert L. Nussbaum and Dr. Nelson B. Cole for providing us the plasmid construct for α-synuclein. We are also grateful to Dr. Malcolm R. Wood for EM technical assistance, to Dr. Peter E. Wright for use of CD spectrometer, to Dr. Julius Rebek, Jr., for use of the VP-ITC instrument, and to Dr. Josephine C. Ferreon and Dr. Jörg Rösgen for helpful communications and critical review of the manuscript.

SUPPORTING INFORMATION AVAILABLE

Figures presenting ITC data for SDS micelle formation in buffer, α-synuclein CD thermal scan data at 1 mM SDS using different protein concentrations, three-state analysis of α-synuclein−monomeric SDS isothermal titration data, and protein CD spectral scan data under different pH conditions in the absence of SDS. This material is available free of charge via the Internet at http://pubs.acs.org.

REFERENCES

1. Maroteaux, L., Campanelli, J. T., and Scheller, R. H. (1988) Synuclein: A neuron-specific protein localized to the nucleus and presynaptic nerve terminal, *J. Neurosci. 8*, 2804−2815.
2. Jakes, R., Spillantini, M. G., and Goedert, M. (1994) Identification of two distinct synucleins from human brain, *FEBS Lett. 345*, 27−32.
3. Weinreb, P. H., Zhen, W., Poon, A. W., Conway, K. A., and Lansbury, P. T., Jr. (1996) NACP, a protein implicated in Alzheimer's disease and learning, is natively unfolded, *Biochemistry 35*, 13709−13715.
4. Polymeropoulos, M. H., Lavedan, C., Leroy, E., Ide, S. E., Dehejia, A., Dutra, A., Pike, B., Root, H., Rubenstein, J., Boyer, R., Stenroos, E. S., Chandrasekharappa, S., Athanassiadou, A., Papapetropoulos, T., Johnson, W. G., Lazzarini, A. M., Duvoisin, R. C., Di Iorio, G., Golbe, L. I., and Nussbaum, R. L. (1997) Mutation in the α-synuclein gene identified in families with Parkinson's disease, *Science 276*, 2045−2047.
5. Kruger, R., Kuhn, W., Muller, T., Woitalla, D., Graeber, M., Kosel, S., Przuntek, H., Epplen, J. T., Schols, L., and Riess, O. (1998) Ala30Pro mutation in the gene encoding α-synuclein in Parkinson's disease, *Nat. Genet. 18*, 106−108.
6. Singleton, A. B., Farrer, M., Johnson, J., Singleton, A., Hague, S., Kachergus, J., Hulihan, M., Peuralinna, T., Dutra, A., Nussbaum, R., Lincoln, S., Crawley, A., Hanson, M., Maraganore, D., Adler, C., Cookson, M. R., Muenter, M., Baptista, M., Miller, D., Blancato, J., Hardy, J., and Gwinn-Hardy, K. (2003) α-Synuclein locus triplication causes Parkinson's disease, *Science 302*, 841.
7. Eriksen, J. L., Dawson, T. M., Dickson, D. W., and Petrucelli, L. (2003) Caught in the act: α-Synuclein is the culprit in Parkinson's disease, *Neuron 40*, 453−456.
8. Dawson, T. M., and Dawson, V. L. (2003) Molecular pathways of neurodegeneration in Parkinson's disease, *Science 302*, 819−822.
9. Nussbaum, R. L., and Ellis, C. E. (2003) Alzheimer's disease and Parkinson's disease, *N. Engl. J. Med. 348*, 1356−1364.
10. Spillantini, M. G., Schmidt, M. L., Lee, V. M., Trojanowski, J. Q., Jakes, R., and Goedert, M. (1997) α-Synuclein in Lewy bodies, *Nature 388*, 839−840.
11. Spillantini, M. G., Crowther, R. A., Jakes, R., Hasegawa, M., and Goedert, M. (1998) α-Synuclein in filamentous inclusions of Lewy bodies from Parkinson's disease and dementia with lewy bodies, *Proc. Natl. Acad. Sci. U.S.A. 95*, 6469−6473.
12. Dev, K. K., Hofele, K., Barbieri, S., Buchman, V. L., and van der Putten, H. (2003) Part II: α-Synuclein and its molecular pathophysiological role in neurodegenerative disease, *Neuropharmacology 45*, 14−44.
13. Rampello, L., Cerasa, S., Alvano, A., Butta, V., Raffaele, R., Vecchio, I., Cavallaro, T., Cimino, E., Incognito, T., and Nicoletti, F. (2004) Dementia with Lewy bodies: A review, *Arch. Gerontol. Geriatr. 39*, 1−14.
14. Ueda, K., Fukushima, H., Masliah, E., Xia, Y., Iwai, A., Yoshimoto, M., Otero, D. A., Kondo, J., Ihara, Y., and Saitoh, T. (1993) Molecular cloning of cDNA encoding an unrecognized component of amyloid in Alzheimer disease, *Proc. Natl. Acad. Sci. U.S.A. 90*, 11282−11286.
15. Abeliovich, A., Schmitz, Y., Farinas, I., Choi-Lundberg, D., Ho, W. H., Castillo, P. E., Shinsky, N., Verdugo, J. M., Armanini, M., Ryan, A., Hynes, M., Phillips, H., Sulzer, D., and Rosenthal, A. (2000) Mice lacking α-synuclein display functional deficits in the nigrostriatal dopamine system, *Neuron 25*, 239−252.
16. Murphy, D. D., Rueter, S. M., Trojanowski, J. Q., and Lee, V. M. (2000) Synucleins are developmentally expressed, and α-synuclein regulates the size of the presynaptic vesicular pool in primary hippocampal neurons, *J. Neurosci. 20*, 3214−3220.
17. Cabin, D. E., Shimazu, K., Murphy, D., Cole, N. B., Gottschalk, W., McIlwain, K. L., Orrison, B., Chen, A., Ellis, C. E., Paylor, R., Lu, B., and Nussbaum, R. L. (2002) Synaptic vesicle depletion correlates with attenuated synaptic responses to prolonged repetitive stimulation in mice lacking α-synuclein, *J. Neurosci. 22*, 8797−8807.
18. Lotharius, J., and Brundin, P. (2002) Impaired dopamine storage resulting from α-synuclein mutations may contribute to the pathogenesis of Parkinson's disease, *Hum. Mol. Genet. 11*, 2395−2407.
19. Chandra, S., Gallardo, G., Fernandez-Chacon, R., Schluter, O. M., and Sudhof, T. C. (2005) α-Synuclein cooperates with CSPα in preventing neurodegeneration, *Cell 123*, 383−396.
20. Perez, R. G., and Hastings, T. G. (2004) Could a loss of α-synuclein function put dopaminergic neurons at risk? *J. Neurochem. 89*, 1318−1324.
21. Leng, Y., and Chuang, D. M. (2006) Endogenous α-synuclein is induced by valproic acid through histone deacetylase inhibition and participates in neuroprotection against glutamate-induced excitotoxicity, *J. Neurosci. 26*, 7502−7512.
22. Cooper, A. A., Gitler, A. D., Cashikar, A., Haynes, C. M., Hill, K. J., Bhullar, B., Liu, K., Xu, K., Strathearn, K. E., Liu, F., Cao, S., Caldwell, K. A., Caldwell, G. A., Marsischky, G., Kolodner, R. D., Labaer, J., Rochet, J. C., Bonini, N. M., and Lindquist, S. (2006) α-Synuclein blocks ER-Golgi traffic and Rab1 rescues neuron loss in Parkinson's models, *Science 313*, 324−328.
23. Uversky, V. N., and Fink, A. L. (2002) Amino acid determinants of α-synuclein aggregation: Putting together pieces of the puzzle, *FEBS Lett. 522*, 9−13.
24. Jao, C. C., Der-Sarkissian, A., Chen, J., and Langen, R. (2004) Structure of membrane-bound α-synuclein studied by site-directed spin labeling, *Proc. Natl. Acad. Sci. U.S.A. 101*, 8331−8336.
25. Davidson, W. S., Jonas, A., Clayton, D. F., and George, J. M. (1998) Stabilization of α-synuclein secondary structure upon binding to synthetic membranes, *J. Biol. Chem. 273*, 9443−9449.
26. Chandra, S., Chen, X., Rizo, J., Jahn, R., and Sudhof, T. C. (2003) A broken α-helix in folded α-synuclein, *J. Biol. Chem. 278*, 15313−15318.
27. Der-Sarkissian, A., Jao, C. C., Chen, J., and Langen, R. (2003) Structural organization of α-synuclein fibrils studied by site-directed spin labeling, *J. Biol. Chem. 278*, 37530−37535.
28. Heise, H., Hoyer, W., Becker, S., Andronesi, O. C., Riedel, D., and Baldus, M. (2005) Molecular-level secondary structure, polymorphism, and dynamics of full-length α-synuclein fibrils studied by solid-state NMR, *Proc. Natl. Acad. Sci. U.S.A. 102*, 15871−15876.
29. Del Mar, C., Greenbaum, E. A., Mayne, L., Englander, S. W., and Woods, V. L., Jr. (2005) Structure and properties of α-synuclein and other amyloids determined at the amino acid level, *Proc. Natl. Acad. Sci. U.S.A. 102*, 15477−15482.
30. Serpell, L. C., Berriman, J., Jakes, R., Goedert, M., and Crowther, R. A. (2000) Fiber diffraction of synthetic α-synuclein filaments shows amyloid-like cross-β conformation, *Proc. Natl. Acad. Sci. U.S.A. 97*, 4897−4902.
31. Hoyer, W., Cherny, D., Subramaniam, V., and Jovin, T. M. (2004) Impact of the acidic C-terminal region comprising amino acids 109−140 on α-synuclein aggregation in vitro, *Biochemistry 43*, 16233−16242.
32. Li, W., West, N., Colla, E., Pletnikova, O., Troncoso, J. C., Marsh, L., Dawson, T. M., Jakala, P., Hartmann, T., Price, D. L., and Lee, M. K. (2005) Aggregation promoting C-terminal truncation of α-synuclein is a normal cellular process and is enhanced by the familial Parkinson's disease-linked mutations, *Proc. Natl. Acad. Sci. U.S.A. 102*, 2162−2167.
33. Bertoncini, C. W., Jung, Y. S., Fernandez, C. O., Hoyer, W., Griesinger, C., Jovin, T. M., and Zweckstetter, M. (2005) Release of long-range tertiary interactions potentiates aggregation of natively unstructured α-synuclein, *Proc. Natl. Acad. Sci. U.S.A. 102*, 1430−1435.
34. Uversky, V. N., Gillespie, J. R., and Fink, A. L. (2000) Why are "natively unfolded" proteins unstructured under physiologic conditions? *Proteins 41*, 415−427.
35. Crowther, R. A., Jakes, R., Spillantini, M. G., and Goedert, M. (1998) Synthetic filaments assembled from C-terminally truncated α-synuclein, *FEBS Lett. 436*, 309−312.
36. Conway, K. A., Harper, J. D., and Lansbury, P. T., Jr. (2000) Fibrils formed in vitro from α-synuclein and two mutant forms linked to Parkinson's disease are typical amyloid, *Biochemistry 39*, 2552−2563.

37. Conway, K. A., Harper, J. D., and Lansbury, P. T. (1998) Accelerated in vitro fibril formation by a mutant α-synuclein linked to early-onset Parkinson disease, *Nat. Med. 4*, 1318−1320.
38. Wood, S. J., Wypych, J., Steavenson, S., Louis, J. C., Citron, M., and Biere, A. L. (1999) α-Synuclein fibrillogenesis is nucleation-dependent. Implications for the pathogenesis of Parkinson's disease, *J. Biol. Chem. 274*, 19509−19512.
39. Uversky, V. N., Li, J., and Fink, A. L. (2001) Evidence for a partially folded intermediate in α-synuclein fibril formation, *J. Biol. Chem. 276*, 10737−10744.
40. Fink, A. L. (2006) The aggregation and fibrillation of α-synuclein, *Acc. Chem. Res. 39*, 628−634.
41. Reynolds, J. A., and Tanford, C. (1970) Binding of dodecyl sulfate to proteins at high binding ratios. Possible implications for the state of proteins in biological membranes, *Proc. Natl. Acad. Sci. U.S.A. 66*, 1002−1007.
42. Reynolds, J. A., and Tanford, C. (1970) The gross conformation of protein-sodium dodecyl sulfate complexes, *J. Biol. Chem. 245*, 5161−5165.
43. Ulmer, T. S., and Bax, A. (2005) Comparison of structure and dynamics of micelle-bound human α-synuclein and Parkinson disease variants, *J. Biol. Chem. 280*, 43179−43187.
44. Ulmer, T. S., Bax, A., Cole, N. B., and Nussbaum, R. L. (2005) Structure and dynamics of micelle-bound human α-synuclein, *J. Biol. Chem. 280*, 9595−9603.
45. Bisaglia, M., Tessari, I., Pinato, L., Bellanda, M., Giraudo, S., Fasano, M., Bergantino, E., Bubacco, L., and Mammi, S. (2005) A topological model of the interaction between α-synuclein and sodium dodecyl sulfate micelles, *Biochemistry 44*, 329−339.
46. Cole, N. B., Murphy, D. D., Grider, T., Rueter, S., Brasaemle, D., and Nussbaum, R. L. (2002) Lipid droplet binding and oligomerization properties of the Parkinson's disease protein α-synuclein, *J. Biol. Chem. 277*, 6344−6352.
47. Gill, S. C., and von Hippel, P. H. (1989) Calculation of protein extinction coefficients from amino acid sequence data, *Anal. Biochem. 182*, 319−326.
48. Edelhoch, H. (1967) Spectroscopic determination of tryptophan and tyrosine in proteins, *Biochemistry 6*, 1948−1954.
49. Pace, C. N., Vajdos, F., Fee, L., Grimsley, G., and Gray, T. (1995) How to measure and predict the molar absorption coefficient of a protein, *Protein Sci. 4*, 2411−2423.
50. Wiseman, T., Williston, S., Brandts, J. F., and Lin, L. N. (1989) Rapid measurement of binding constants and heats of binding using a new titration calorimeter, *Anal. Biochem. 179*, 131−137.
51. Helenius, A., McCaslin, D. R., Fries, E., and Tanford, C. (1979) Properties of detergents, *Methods Enzymol. 56*, 734−749.
52. Otzen, D. E. (2002) Protein unfolding in detergents: Effect of micelle structure, ionic strength, pH, and temperature, *Biophys. J. 83*, 2219−2230.
53. Kuznetsova, I. M., Turoverov, K. K., and Uversky, V. N. (2004) Use of the phase diagram method to analyze the protein unfolding-refolding reactions: Fishing out the "invisible" intermediates, *J. Proteome Res. 3*, 485−494.
54. Myers, J. K., Pace, C. N., and Scholtz, J. M. (1995) Denaturant m values and heat capacity changes: Relation to changes in accessible surface areas of protein unfolding, *Protein Sci. 4*, 2138−2148.
55. Rosgen, J., and Hinz, H. J. (2003) Phase diagrams: A graphical representation of linkage relations, *J. Mol. Biol. 328*, 255−271.
56. Ferreon, A. C., Ferreon, J. C., Bolen, D. W., and Rosgen, J. (2007) Protein phase diagrams II: Nonideal behavior of biochemical reactions in the presence of osmolytes, *Biophys. J. 92*, 245−256.
57. Gudiksen, K. L., Gitlin, I., and Whitesides, G. M. (2006) Differentiation of proteins based on characteristic patterns of association and denaturation in solutions of SDS, *Proc. Natl. Acad. Sci. U.S.A. 103*, 7968−7972.
58. Otzen, D. E., and Oliveberg, M. (2002) Burst-phase expansion of native protein prior to global unfolding in SDS, *J. Mol. Biol. 315*, 1231−1240.
59. de Laureto, P. P., Tosatto, L., Frare, E., Marin, O., Uversky, V. N., and Fontana, A. (2006) Conformational properties of the SDS-bound state of α-synuclein probed by limited proteolysis: Unexpected rigidity of the acidic C-terminal tail, *Biochemistry 45*, 11523−11531.
60. Jo, E., McLaurin, J., Yip, C. M., St George-Hyslop, P., and Fraser, P. E. (2000) α-Synuclein membrane interactions and lipid specificity, *J. Biol. Chem. 275*, 34328−34334.
61. Munishkina, L. A., Phelan, C., Uversky, V. N., and Fink, A. L. (2003) Conformational behavior and aggregation of α-synuclein in organic solvents: Modeling the effects of membranes, *Biochemistry 42*, 2720−2730.
62. Fernandez, P., Schrodle, S., Buchner, R., and Kunz, W. (2003) Micelle and solvent relaxation in aqueous sodium dodecylsulfate solutions, *ChemPhysChem 4*, 1065−1072.
63. Bussell, R., Jr., and Eliezer, D. (2003) A structural and functional role for 11-mer repeats in α-synuclein and other exchangeable lipid binding proteins, *J. Mol. Biol. 329*, 763−778.
64. Dobson, C. M. (2003) Protein folding and misfolding, *Nature 426*, 884−890.
65. Lashuel, H. A., Hartley, D., Petre, B. M., Walz, T., and Lansbury, P. T., Jr. (2002) Neurodegenerative disease: Amyloid pores from pathogenic mutations, *Nature 418*, 291.
66. Lashuel, H. A., Petre, B. M., Wall, J., Simon, M., Nowak, R. J., Walz, T., and Lansbury, P. T., Jr. (2002) α-Synuclein, especially the Parkinson's disease-associated mutants, forms pore-like annular and tubular protofibrils, *J. Mol. Biol. 322*, 1089−1102.
67. Lashuel, H. A., and Lansbury, P. T. (2006) Are amyloid diseases caused by protein aggregates that mimic bacterial pore-forming toxins? *Q. Rev. Biophys.*, 1−35.
68. Volles, M. J., and Lansbury, P. T., Jr. (2003) Zeroing in on the pathogenic form of α-synuclein and its mechanism of neurotoxicity in Parkinson's disease, *Biochemistry 42*, 7871−7878.

BI602461Y